Design of diamond-shape photonic crystal fiber polarization filter based on surface plasma resonance effect[*]

Yongxia Zhang(张永霞)[1], Jinhui Yuan(苑金辉)[1,2,†], Yuwei Qu(屈玉玮)[2], Xian Zhou(周娴)[1],
Binbin Yan(颜玢玢)[2], Qiang Wu(吴强)[3], Kuiru Wang(王葵如)[2], Xinzhu Sang(桑新柱)[2],
Keping Long(隆克平)[1], and Chongxiu Yu(余重秀)[2]

[1]*Research Center for Convergence Networks and Ubiquitous Services, University of Science and Technology Beijing (USTB), Beijing* 100083, *China*
[2]*State Key Laboratory of Information Photonics and Optical Communications, Beijing University of Posts and Telecommunications, Beijing* 100876, *China*
[3]*Department of Physics and Electrical Engineering, Northumbria University, Newcastle upon Tyne, NE*1 8*ST, United Kingdom*

A novel plasmonic polarization filter based on the diamond-shape photonic crystal fiber (PCF) is proposed. The resonant coupling characteristics of the PCF polarization filter are investigated by the full-vector finite-element method. By optimizing the geometric parameters of the PCF, when the fiber length is 5 mm, the polarization filter has a bandwidth of 990 nm and an extinction ratio (ER) of lower than -20 dB. Moreover, a single wavelength polarization filter can also be achieved, along with an ER of -279.78 dB at wavelength 1.55 μm. It is believed that the proposed PCF polarization filter will be very useful in laser and optical communication systems.

1. Introduction

Photonic crystal fibers (PCFs) have been attracting great interest due to their unique optical properties such as adjustable dispersion,[1–4] high nonlinearity,[5] and large birefringence.[6–9] When the light is propagated inside PCFs coated with the metal films or filled with the metal wires, the free electrons on the metal surface interact with the incident light field, forming the surface plasma resonance (SPR).[10] The PCF polarization-related devices based on the SPR effect have potential applications in many fundamental and applied sciences.[11–18] The PCF polarization filter is one of the most important devices.

In 2007, Zhang *et al.*[19] selectively coated a silver film on the PCF holes using the chemical vapor deposition method. In 2008, Lee *et al.*[20] proposed the melt-filling gold technology to fill a gold wire into the PCF air hole. After that, many research works are concentrated on the PCFs which are filled or coated with different metals,[21–24] and the PCF polarization filter based on the SPR effect becomes feasible. In 2013, Xue *et al.*[25] reported an SPR-based PCF polarization filter, in which the confinement loss of the *y*-polarized core mode at wavelength 1.31 μm was 508 dB/cm. In 2015, Liu *et al.*[26] demonstrated a broadband PCF polarization filter based on the SPR effect, whose bandwidth was up to 430 nm. In 2017, Li *et al.* achieved a dual-wavelength PCF polarization filter, whose confinement losses induced by the SPR effect were 265.04 dB/cm and 230.5 dB/cm at wavelengths 1.31 μm and 1.55 μm, respectively.[27] In 2018, Wang *et al.*[28] reported a broadband PCF polarization filter with a large diameter gold-coated air hole, whose bandwidth covers the whole communication wave band.

In this paper, a novel plasmonic polarization filter based on the diamond-shape PCF is proposed. The confinement loss and resonant coupling characteristics of the proposed PCF polarization filter are investigated, and the influences of the fiber geometric parameters on the confinement loss are analyzed. By adjusting the fiber geometric parameters, a single wavelength polarization filter with an extinction ratio (ER) of -279.78 dB at wavelength 1.55 μm is achieved.

2. The PCF design and theory

Figure 1 shows the schematic diagram of the proposed PCF polarization filter. The PCF cladding has four layers of air holes, which are arranged in a diamond shape. The spacing between the adjacent holes in the *x* and *y* directions are Λ_x and Λ_y, respectively. The constant $\Lambda_y = 2.4$ μm. The diameter of the air hole with the gold-coated film is d_1, and the thickness of the gold film is t. The two large air holes with the diameter of d_2 along the *y* direction are used to introduce the birefringence. A perfect matching layer (PML) and the scattering boundary condition are used at the outermost layer to reduce the energy loss.

The full-vector finite-element method is employed to investigate the coupling characteristics of the designed PCF polarization filter between the core mode and surface plasma polariton (SPP) modes. Because of the air hole coated with the

[†]Corresponding author. E-mail: yuanjinhui81@bupt.edu.cn

gold film, the core-guided mode occurs to resonate with the SPP modes at some specific wavelengths, resulting in large confinement loss of the core mode. The confinement loss L_C can be described as following:[29]

$$L_C = \frac{20}{\ln 10} \frac{2\pi}{\lambda} \text{Im}[n_{\text{eff}}] \times 10^6, \qquad (1)$$

where λ is the operating wavelength of light, and $\text{Im}[n_{\text{eff}}]$ is the imaginary part of effective refractive index.
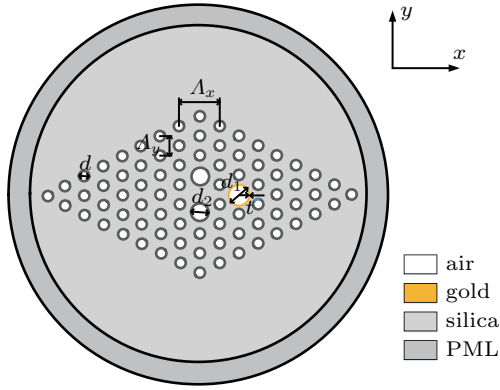

Fig. 1. The schematic diagram of the proposed PCF polarization filter.

The background material of the proposed PCF polarization filter is the silica, whose material dispersion can be obtained from the Sellmeier equation.[30] In the visible and near-infrared spectral regions, the material dispersion of the gold film can be calculated using the Drude–Lorentz model[31]

$$\varepsilon_{\text{m}} = \varepsilon_{\infty} - \frac{\omega_{\text{D}}^2}{\omega(\omega - \text{j}\gamma_{\text{D}})} - \frac{\Delta\varepsilon \cdot \Omega_{\text{L}}^2}{(\omega^2 - \Omega_{\text{L}}^2) - \text{j}\Gamma_{\text{L}}\omega}, \qquad (2)$$

where ε_{m} is the dielectric constant of the gold, ε_{∞} is the dielectric constant at the high frequency, Δ_{ε} is the weighting factor, ω_{D} and γ_{D} represent the plasma frequency and damping frequency, ω is the angle frequency of guided-light, and Ω_{L} and Γ_{L} are the frequency and spectral width of the Lorentz oscillator.

The ER is an important parameter for evaluating the performance of the PCF polarization filter. The ER can be calculated as follows:[32]

$$\text{ER} = 10\log_{10}\frac{P_{\text{out}}(x)}{P_{\text{out}}(y)}, \qquad (3)$$

where $P_{\text{out}}(x)$ and $P_{\text{out}}(y)$ stand for the x- and y-polarized output powers.

3. Simulation results and analysis

Figure 2(a) shows the real part of the effective refractive indices ($\text{Re}(n_{\text{eff}})$) of the core mode and x-polarized SPP modes when the geometric parameters of PCF are set as $d = 1.30$ μm, $d_1 = 2.75$ μm, $d_2 = 2.65$ μm, $\Lambda_x = 4.0$ μm, and $t = 48$ nm, respectively. From Fig. 2(a), the phase-matching

condition at wavelengths 1.33 and 1.56 μm is satisfied, and the x-polarized core mode occurs to resonant with the 3rd- and 2nd-order SPP modes, respectively. Here $\text{Re}(n_{\text{eff}})$ values of the 0th-order and 1st-order SPP modes are much higher than that of the core mode, so they cannot be coupled into the core region. Figure 2(b) shows the confinement losses of the x- and y-polarized core modes. The insets of Fig. 2(b) show the electric field distributions of the core modes at different wavelengths. At the phase-matching wavelengths 1.33 μm and 1.56 μm, the energy of the x-polarized core mode leaks a lot to the surface of the metal film, stimulating the SPR effect. This results in a great confinement loss in the x-polarized core mode over the operating wavelength range, as seen from Fig. 2(b). Moreover, the confinement loss of the x-polarized is much larger than that of the y-polarized core mode, and the strong resonance coupling between the x-polarized core mode and SPP modes occurs, while the energy of the y-polarized core mode is mainly confined in the core region due to the weak resonance. This is because the air hole with the gold-coated film is distributed in the x direction of the PCF cladding.
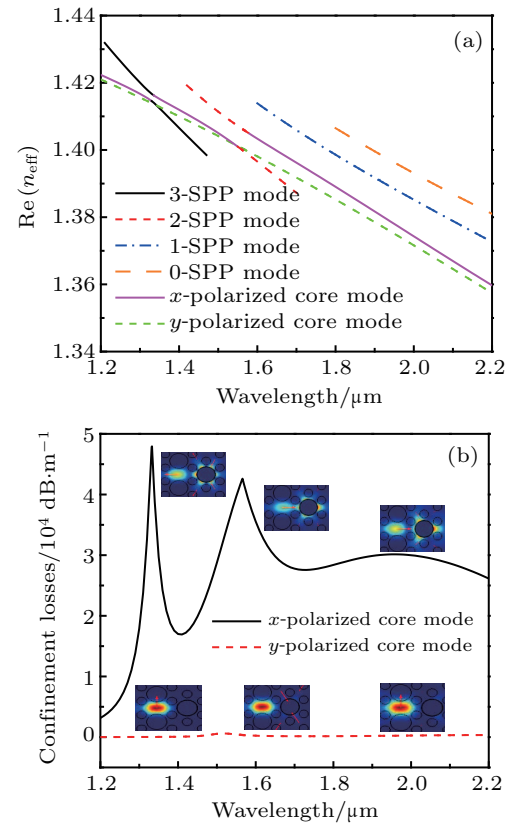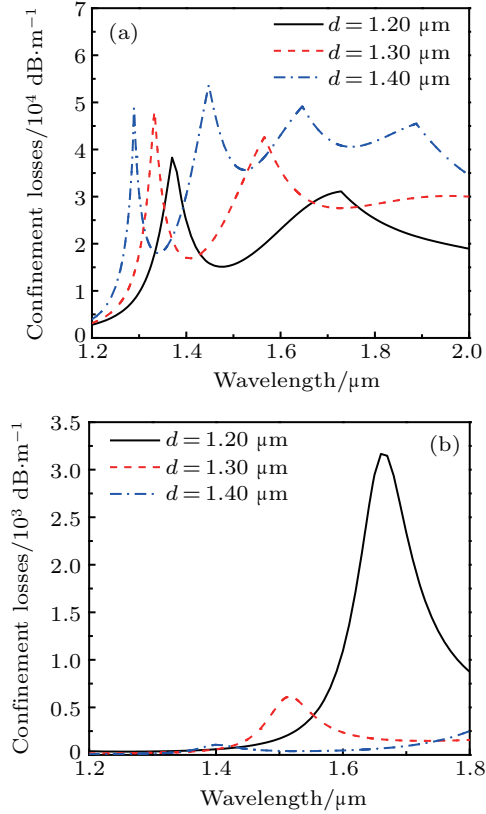

Fig. 2. (a) The real part of the effective refractive indices of the core modes and the x-polarized SPP modes, and (b) the confinement losses of the x- and y-polarized core modes. The insets showing the electric field distributions of the core modes at different wavelengths.
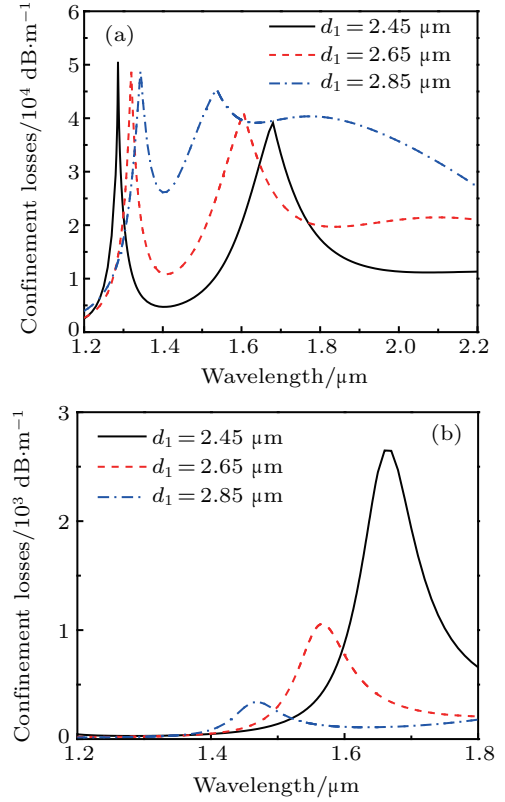
In the following, some geometric parameters of PCF including d, d_1, d_2, Λ_x, and t are adjusted in order to investigate the coupling characteristic. The variations of the confinement loss of the x- and y-polarized with different d are shown in Figs. 3(a) and 3(b), respectively. As d increases

from 1.2 μm to 1.4 μm, $Re(n_{eff})$ of the core modes and SPP modes decreases gradually, so the resonant wavelength of the x-polarized core mode occurs to shift toward the shorter wavelength. From Fig. 3(a), as d increases, the resonant coupling strength between the x-polarized core mode and SPP modes is enhanced, resulting in an increase of the confinement loss peak of the x-polarized core mode. From Fig. 3(b), because the resonant coupling strength between the y-polarized core mode and SPP mode decreases as d increases from 1.2 μm to 1.4 μm, the confinement loss of the y-polarized core mode decreases.
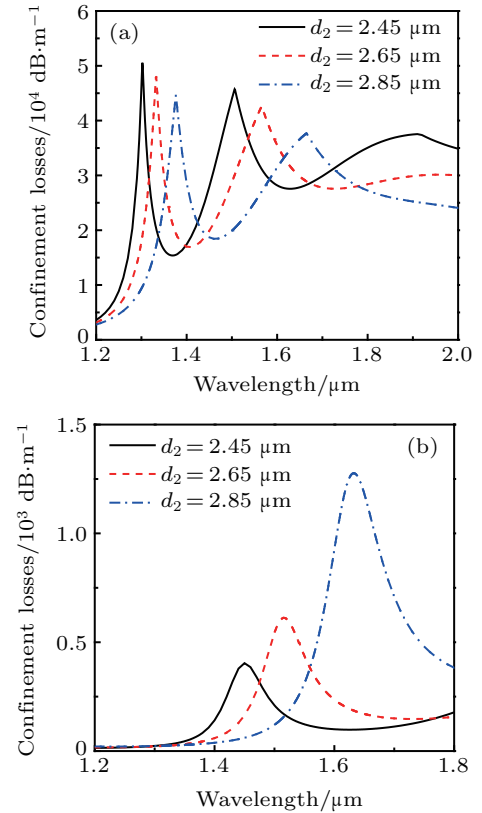

Fig. 3. The variations of the confinement loss of (a) the x-polarized core mode and (b) the y-polarized core mode with different d.

The variations of the confinement loss of the x- and y-polarized core modes with different values of d_1 are shown in Figs. 4(a) and 4(b), respectively. From Fig. 4(a), as d_1 increases from 2.45 μm to 2.85 μm, $Re(n_{eff})$ of the 2nd- and 3rd-order SPP mode decreases and increases, and resonant wavelengths of the x-polarized and y-polarized core modes are redshifted and blue-shifted, respectively. When d_1 increases, the distance between the core region and gold film is decreased, the resonance coupling effect is enhanced, and the confinement loss of the x-polarized is increased. From Fig. 4(b), as d_1 increases from 2.45 μm to 2.85 μm, the resonant wavelength of the y-polarized core mode is blue-shifted. As d_1 increases, $Re(n_{eff})$ of the core region is nearly unchanged, while $Re(n_{eff})$ of the y-polarized SPP mode increases. At this time, the coupling strength between the y-polarized core mode and SPP mode decreases, so the confinement loss peak of the y-polarized core mode decreases.
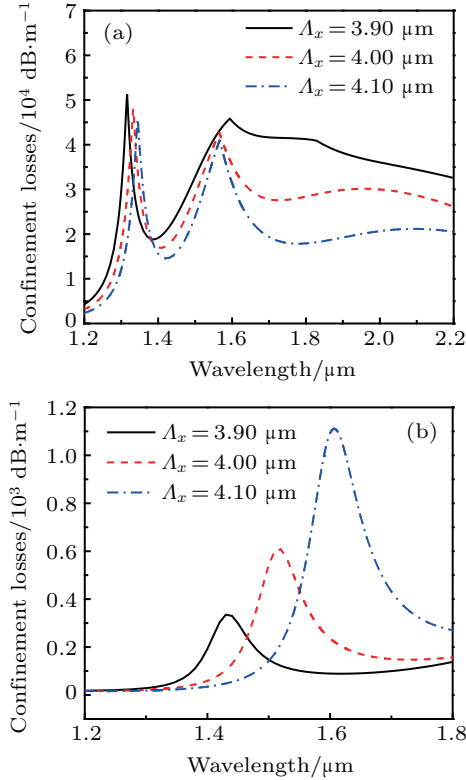

Fig. 4. The variations of the confinement loss of (a) the x-polarized core mode and (b) the y-polarized core mode with different d_1.

Fig. 5. The variations of the confinement loss of (a) the x-polarized core mode and (b) the y-polarized core mode with different d_2.

The variations of the confinement loss of the x- and y-polarized core modes with different values of d_2 are shown in Figs. 5(a) and 5(b), respectively. As d_2 increases from 2.45 μm
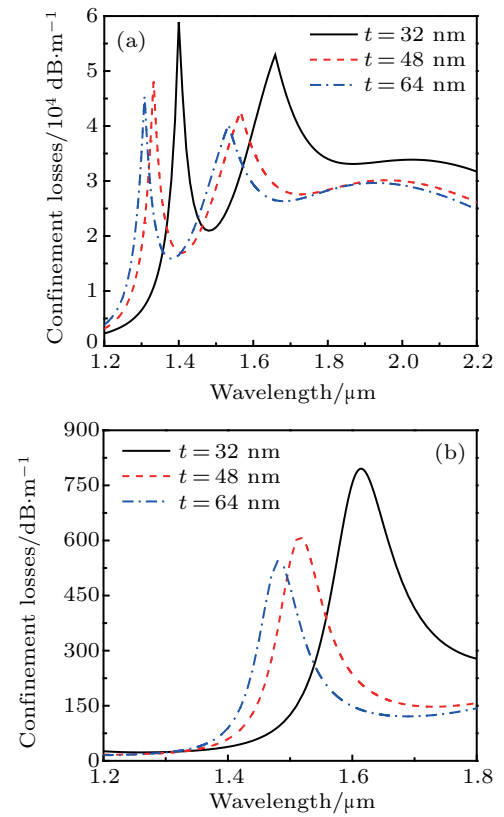
to 2.85 μm, Re(n_{eff}) of the x-polarized and y-polarized core modes decreases, while Re(n_{eff}) of the SPP modes increases. It is obvious that the resonant wavelengths of both the x-polarized and y-polarized core modes are red-shifted. With the increase of d_2, the confinement loss of the x-polarized core mode decreases. From Fig. 5(b), as d_2 increases from 2.45 μm to 2.85 μm, the core region gradually decreases, the constraint on the y-polarized core mode becomes weaker, and the coupling strength between the y-polarized core mode and the SPP mode increases, so the confinement loss of the y-polarized core mode increases.

Fig. 6. The variations of the confinement loss of (a) the x-polarized core mode and (b) the y-polarized core mode for different Λ_x.

The variations of the confinement loss of the x- and y-polarized core modes with different values of Λ_x are shown in Figs. 6(a) and 6(b), respectively. As Λ_x increases from 3.9 μm to 4.1 μm, Re(n_{eff}) of the x-polarized and y-polarized core modes and SPP modes increases. From Fig. 6(a), the resonant wavelengths between the x-polarized core mode and 1st- and 3rd-order SPP modes occur to red-shift, and the resonant wavelength between the x-polarized core mode and 2nd-order SPP mode occurs to blue-shift. As Λ_x increases from 3.9 μm to 4.1 μm, the distance between the core region and gold film increases, resulting in the reduction of the confinement loss of the x-polarized core mode. From Fig. 6(b), as Λ_x increases from 3.9 μm to 4.1 μm, the resonant wavelength of the y-polarized core mode occurs to red-shift, and the leakage channel between the air holes becomes larger. Thus, the coupling strength between the y-polarized core mode and SPP mode increases, resulting in the increase in the confinement loss of the y-polarized core mode.
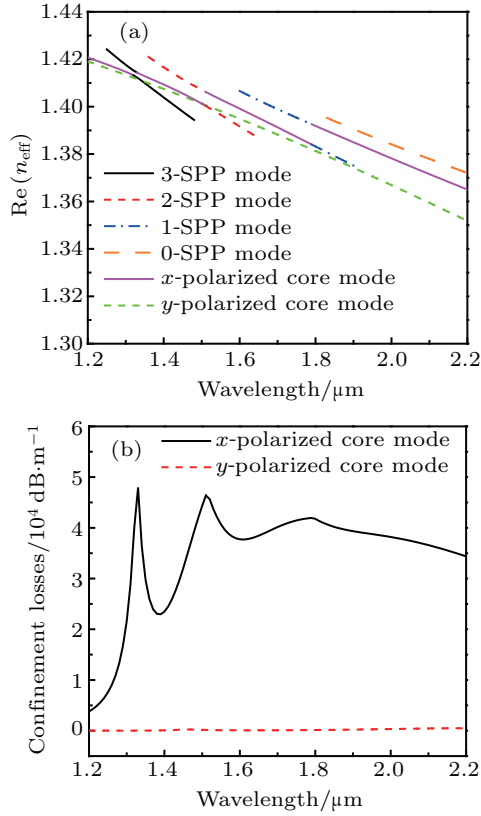
The variations of the confinement loss of the x- and y-polarized core modes with different values of t are shown in Figs. 7(a) and 7(b), respectively. As t increases from 32 nm to 64 nm, Re(n_{eff}) of the SPP modes decreases greatly, while the change of t has no effect on Re(n_{eff}) of the core mode. The resonant wavelengths of the x-polarized and y-polarized core modes are blue-shifted. It is worth noting that the confinement losses of the x-polarized and y-polarized core modes decrease as t increases. When t increases from 32 nm to 64 nm, the energy of the x-polarized and y-polarized core mode penetrates inside the gold layer, and the energy of the SPP modes inside the inner layer of the gold film decreases. Therefore, the resonant coupling strength becomes weaker, resulting in a reduction in the confinement loss of the x-polarized and y-polarized core modes.

Fig. 7. The variations of the confinement loss of (a) the x-polarized core mode and (b) the y-polarized core mode for different t.

A broadband PCF polarization filter could be achieved by optimizing the fiber geometric parameters. Figure 8(a) shows Re(n_{eff}) of the x-polarized and y-polarized core modes and SPP modes when the fiber geometric parameters are chosen as follows: $d = 1.35$ μm, $d_1 = 2.80$ μm, $d_2 = 2.75$ μm, $\Lambda_x = 4.0$ μm, and $t = 50$ nm. The x-polarized core mode occurs to intersect with the 3rd-, 2nd-, and 1st-order SPP modes at wavelengths 1.33 μm, 1.51 μm, and 1.79 μm, respectively, where the phase-matching condition is satisfied. Here Re(n_{eff}) of the 0th-order SPP mode is much higher than that of the core mode, so the resonance coupling cannot occur. Figure 8(b) shows the confinement losses of the x-polarized and y-polarized core modes. It can be seen from

Fig. 8(b) that the confinement loss of the x-polarized core mode is much greater than that of the y-polarized core mode. At wavelengths 1.31 μm and 1.55 μm, the confinement losses of the x-polarized core mode are up to 28864.9 dB/m and 40664.51 dB/m, respectively, and the corresponding confinement losses of the y-polarized core mode are only 18.7 dB/m and 99.2 dB/m, respectively.
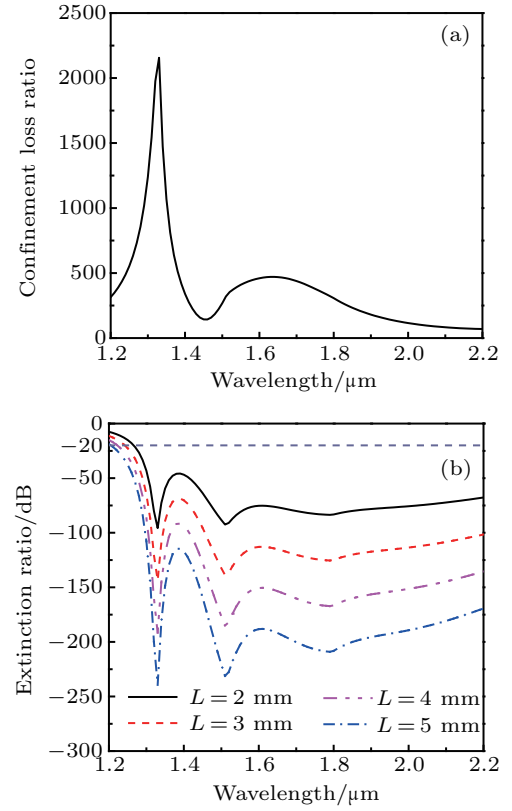

Fig. 8. (a) The real part of the effective refractive indices of the x- and y-polarized core modes and SPP modes, and (b) the confinement losses of the x- and y-polarized core modes.

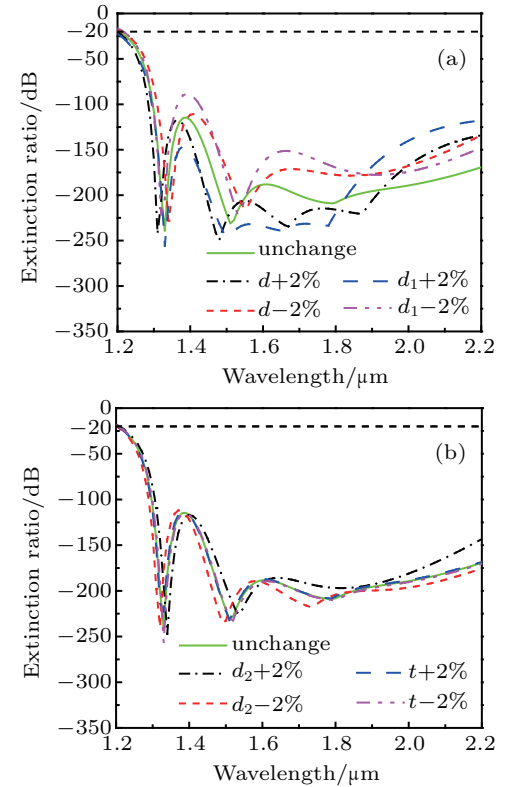The confinement loss ratio, which is defined as the ratio of the confinement loss of the x-polarized core mode to the confinement loss of the y-polarized core mode, is used to evaluate the performance of the PCF polarization filter. Figure 9(a) shows the relationship between the confinement loss ratio and wavelength. From Fig. 9(a), the confinement loss ratio is larger than 100, and the maximum value can be up to 2156.14 at wavelength 1.33 μm. Figure 9(b) shows the relationship between the ER and wavelength when the fiber length L is changed from 2 mm, to 3 mm, to 4 mm, and to 5 mm, respectively. From Fig. 9(b), when L is 5 mm, the ER is less than −20 dB within the wavelength range from 1.21 μm to 2.20 μm. Thus, a broadband PCF polarization filter is achieved.

The PCF could be fabricated by some existing methods, such as stack and draw method, ultrasonic drilling, extrusion and surfacing.[33–35] Then the gold film can be plated in a pore by high pressure chemical vapor deposition method.[36] In the fabrication process, the error tolerances are analyzed. Figures 10(a) and 10(b) show the ER when d, d_1, d_2, and t have

the deviations of ±2%. From Figs. 10(a) and 10(b), when L is 5 mm, the minimum bandwidth is 980 nm, covering from 1220 nm to 2200 nm. Thus, the PCF polarization filter proposed in this paper has good tolerance performance.

Fig. 9. (a) The confinement loss ratio of the x-polarized core mode to the y-polarized core mode. (b) The variations of the ER with different L.
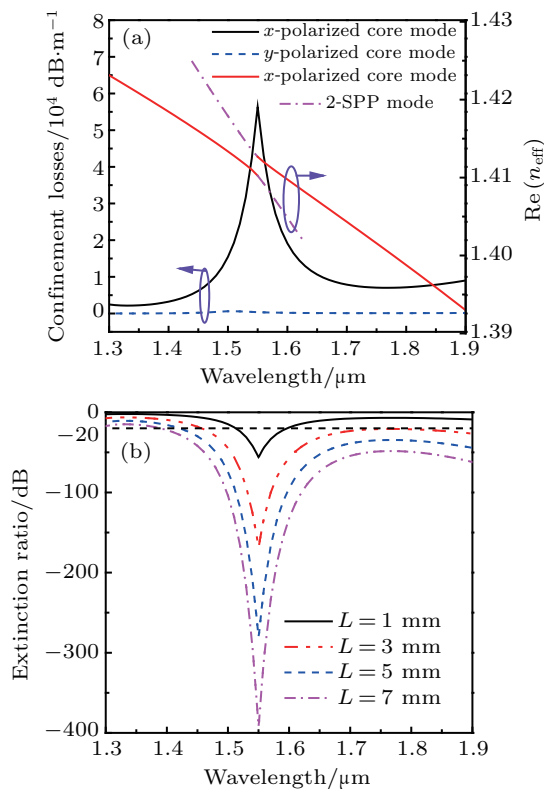

Fig. 10. The variations of the ER when (a) d, d_1 and (b) d_2, t have deviations of ±2%.

4. Single wavelength PCF polarization filter

When the fiber geometric parameters are chosen as follows: $d = 1.36$ μm, $d_1 = 2.35$ μm, $d_2 = 1.99$ μm, $\Lambda_x = 4.0$ μm, and $t = 42$ nm, a single wavelength PCF polarization filter at wavelength 1.55 μm can be achieved. Figure 11(a) shows the confinement losses of the x-polarized and y-polarized core modes and Re(n_{eff}) of the x-polarized core mode and second-order SPP mode. The confinement loss of the x-polarized core mode at resonant wavelength 1.55 μm can reach 56329.4 dB/m, while the corresponding loss of the y-polarized is only 374.6 dB/m. The full width at half maximum is only 40 nm. Figure 11(b) shows the relationships between the ER and wavelength for different L. From Fig. 11(b), when L is 5 mm, the ER can be up to -279.78 dB at wavelength 1.55 μm.

Fig. 11. (a) The confinement losses of the x-polarized and y-polarized core modes and the real part of the effective refractive indices of the x-polarized core mode and 2nd-order SPP mode. (b) The variations of ER with different L.

5. Conclusion

In summary, a plasmonic polarization filter based on the diamond-shape PCF is proposed. By optimizing the fiber geometric parameters, the polarization filter has a bandwidth of 990 nm and an ER of lower than -20 dB. Moreover, a single wavelength PCF polarization filter at wavelength 1.55 μm can be obtained. The confinement loss of the x-polarized core mode can be up to 56329.4 dB/m at wavelength 1.55 μm, where the confinement loss of the y-polarized core mode is only 374.6 dB/m. The proposed polarization filter has the advantages of large bandwidth, high ER, and short length, so it can be widely used in the laser and optical communication systems.

References

[1] Kim S and Kee C 2009 *Opt. Express* **17** 15885
[2] Aliramezani M and Nejad S 2010 *Opt. Laser Technol.* **42** 1209
[3] Fujisawa T, Saitoh K, Wada K and Koshiba M 2006 *Opt. Express* **14** 893
[4] Reeves W, Knight J, Russell P and Roberts P 2002 *Opt. Express* **10** 609
[5] Broderick N, Monro T, Bennett P and Richardson D 1999 *Opt. Lett.* **24** 1395
[6] Yang T Y, Wang E L, Jiang H M, Hu Z J and Xie K 2015 *Opt. Express* **23** 8329
[7] Ademgil H and Haxha S 2008 *J. Lightwave Technol.* **26** 441
[8] Abdelaziz I, AbdelMalek F, Haxha S, Ademgil H and Bouchriha H 2013 *J. Lightwave Technol.* **31** 343
[9] Lu S, Li W, Guo H and Lu M 2011 *Appl. Opt.* **50** 5798
[10] Otto 1968 *Z. Phys. A* **216** 398
[11] Jiang L H, Zheng Y, Yang J J, Hou L T, Li Z H and Zhao X T 2017 *Plasmon* **12** 411
[12] Chen H L, Li S G, Ma M J, Liu Y C, Shi M, Liu Q and Cheng T L 2016 *J. Light. Technol.* **34** 4972
[13] Wang Y, Huang Q, Zhu W J, Yang M H and Lewis E 2018 *Opt. Express* **26** 1910
[14] Wu T S, Shao Y, Wang Y, Cao S Q, Cao W P, Zhang F, Liao C R, He J, Huang Y J, Hou M X and Wang Y P 2017 *Opt. Express* **25** 20313
[15] Zhou X, Li S G, Cheng T L and An G W 2018 *Opt. Quantum Electron.* **50** 157
[16] Liu C, Wang L Y, Yang L, Wang F M, Xu C H, Lv J W, Fu G F, Li X L and Liu Q 2019 *Phys. Lett. A* **383** 3200
[17] Fan Z K, Fang S B, Li S G and Wei Z Y 2019 *Chin. Phys. B* **28** 094209
[18] Wang D D, Mu C L, Kong D P and Guo C Y 2019 *Chin. Phys. B* **28** 118701
[19] Zhang X, Wang R, Cox F, Kuhlmey B and Large M 2007 *Opt. Express* **15** 16270
[20] Lee H W, Schmidt M A, Tyagi H, Sempere and Prill L 2008 *Appl. Phys. Lett.* **93** 111102
[21] Guo Y, Li J S, Li S G, Zhang S H and Liu Y D 2018 *Appl. Opt.* **57** 8016
[22] Chang M, Li B X, Chen N, Lu X L, Zhang X D and Xu J 2019 *IEEE Photon. J.* **11** 7202312
[23] Wang J S, Pei L, Wng S J, Wu L Y, Li J and Ning T G 2018 *Appl. Opt.* **57** 3847
[24] Zhang Z J, Tsuji Y and Eguchi M 2014 *J. Lightwave Technol.* **32** 4558
[25] Xue J R, Li S G, Xiao Y Z, Qin W, Xin X J and Zhu X P 2013 *Opt. Express* **21** 13733
[26] Liu Q, Li S G, Li H, Zi J C, Zhang W, Fan Z K, An G W and Bao Y J 2015 *Plasmon* **10** 931
[27] Li B Y, Li M Q, Peng L, Zhou G Y, Hou Z Y and Xia C M 2017 *IEEE Photon. J.* **9** 5700209
[28] Wang X Y, Li S G, Liu Q and Fan Z K 2018 *Optik* **156** 463
[29] Heikal A, Hussain F, Hameed M and Obayya S 2015 *J. Lightwave Technol.* **33** 2868
[30] Islam M, Sultana J, Rifat A, Dinoviser A, Ng B, Ebendorff-Heideprien H and Abbott D 2018 *Opt. Express* **26** 30347
[31] Liu Q, Li S G and Chen H L 2019 *IEEE Photon. J.* **7** 2700210
[32] Qu Y W, Yuan J H, Zhou X, Li F, Mei C, Yan B B, Wu Q, Wang K R Sang X Z, Long K P and Yu C X 2019 *Opt. Commun.* **452** 1
[33] Feng X, Du H, Li S G, Zhang Y N, Liu Q and Guo X Y 2017 *Opt. Quant. Electron.* **49** 235
[34] Zi J C, Li S G, An G W and Fan Z K 2016 *Opt. Commun.* **363** 80
[35] Xu Z L, Li X Y, Ling W W, Liu P and Zhang Z Y 2015 *Opt. Commun.* **354** 314
[36] An G W, Li S G, Zhang W, Fan Z K and Bao Y J 2014 *Opt. Commun.* **331** 316